Progress In Electromagnetics Research B, Vol. 42, 245–262, 2012

SPACE-TIME ADAPTIVE PROCESSING BASED ON WEIGHTED REGULARIZED SPARSE RECOVERY

Z. C. Yang*, X. Li, and H. Q. Wang

Electronics Science and Engineering School, National University of Defense Technology, Changsha 410073, China

Abstract—In this paper, novel space-time adaptive processing algorithms based on sparse recovery (SR-STAP) that utilize weighted l_1-norm penalty are proposed to further enforce the sparsity and approximate the original l_0-norm. Because the amplitudes of the clutter components from different snapshots are random variables, we design the corresponding weights according to two different ways, i.e., the Capon's spectrum using limited snapshots and the Fourier spectrum using the current snapshot. Moreover, we apply the weighted idea to both the direct data domain (D3) SR-STAP and SR-STAP using multiple snapshots from adjacent target-free range bins. Simulation results illustrate that our proposed algorithms outperform the existing SR-STAP and D3SR-STAP algorithms.

1. INTRODUCTION

By performing a joint-domain optimization of the spatial and temporal degrees-of-freedom (DOFs), space-time adaptive processing (STAP) can improve small target detection in strong ground clutter returns [1–3]. However, there are many practical limitations preventing the use of the optimum STAP processor. One of them is the requirement of a large number of independent and identically distributed (IID) training samples to estimate the interference covariance matrix, which becomes even more serious in non-stationary and nonhomogeneous interference environments [2–4].

Recently, motivated by sparse representaton/sparse recovery (SR) techniques used in radar [5–8], several authors have considered SR ideas for moving target indication (MTI) and STAP problems, such as sparse-recovery-based STAP type (SR-STAP) algorithms in [9–15],

Received 18 May 2012, Accepted 16 July 2012, Scheduled 17 July 2012

* Corresponding author: Zhao Cheng Yang (yangzhaocheng@gmail.com).

L1-regularized STAP filters in [16, 17], etc.. The basic idea of SR-STAP type algorithms is to regularize a linear inverse problem by including prior knowledge that the clutter spectrum is sparse in the angle-Doppler plane. A global matched filter (GMF) is applied to the basic STAP problem, which points out that it has the advantage of being able to work on a single snapshot without prior estimation of the interference matrix since the GMF identifies both the targets and a model of the clutter [9]. Under the assumption of the known clutter ridge in angle-Doppler plane, the authors in [10] imposed a sparse regularization based on l_1-norm penalty to estimate the clutter covariance by excluding the clutter ridge. In [11], the authors presented a post-processing step after clutter whitening using a standard STAP technique by applying sparse regularization. To reduce the need for secondary data or for accurate prior knowledge of the clutter statistics, an iterative adaptive approach (IAA) is presented to compute the clutter covariance matrix in [12]. Unlike the above approaches to directly form the angle-Doppler imaging, the authors in [13–15] tried to estimate the interference covariance matrix using the SR techniques first. The Capon's optimal filter was then constructed with the estimated interference covariance matrix to suppress the clutter. Compared with conventional STAP algorithms, the SR-STAP type algorithms provide high-resolution of the clutter spectrum estimate and exhibit significantly better performance in a very small number of snapshots.

In this paper, we propose a new SR-STAP algorithm that utilizes weighted l_1-norm penalty to obtain a better approximation of l_0-norm and further enforce the sparsity. Motivated by designing the penalty weights using the Capon spectrum to estimate the target's DOA in [19] and considering the situation of IID samples limited in the nonhomogeneous environments, we first simply modify this idea using the diagonal loading technique to estimate the Capon's spectrum, use that to form the l_1-norm penalty weights and apply it to the STAP problem. But this kind of approach requires a matrix inverse resulting in a high computational complexity to form the l_1-norm penalty weights. Thus, we design the corresponding weights for each snapshot according to its own Fourier spectrum calculated by the current snapshot instead of the Capon's spectrum, which results in a lower computational complexity. Furthermore, we apply the weighted idea to both the direct data domain (D3) SR-STAP and SR-STAP using multiple snapshots from adjacent range bins. Numerical simulations are performed to evaluate the performance of our proposed algorithms. The following parts of this paper are organized as: the signal model of STAP in airborne radar systems is first introduced

in Section 2. Section 3 details the proposed weighted SR-STAP algorithms. Section 4 accesses the performance of the proposed algorithms by showing the signal-to-interference ratio (SINR), and detection performance with simulated data. Section 5 provides the summary and conclusions.

2. SIGNAL MODEL

In airborne radar systems, a general model for the space-time clutter plus noise snapshot $\mathbf{x}$ is given by [1]

$$\mathbf{x} = \mathbf{x}_c + \mathbf{n} = \sum_{m=1}^{N_a} \sum_{n=1}^{N_c} \sigma_{m,n} \mathbf{v}(\phi_{m,n}, f_{m,n}) + \mathbf{n}, \tag{1}$$

where $\mathbf{n}$ is the Gaussian white thermal noise vector with the noise power σ_n^2 on each channel and pulse; N_a is the number of range ambiguities; N_c is the number of independent clutter patches over the iso-range of interest; $\phi_{m,n}$ is the angle-of-arrival (AOA) of the mnth clutter patch; $f_{m,n}$ is the corresponding Doppler frequency; $\sigma_{m,n}$ is the complex amplitude for the mnth clutter patch with each element proportional to the square-root of the clutter patches' clutter-noise-ratio (CNR); and $\mathbf{v}(\phi_{m,n},\ f_{m,n})$ is the $NM \times 1$ space-time steering vector for the clutter patch with the AOA $\phi_{m,n}$ and the Doppler frequency $f_{m,n}$. Here, N is the number of pulses in a coherent process interval (CPI) and M is the number of array channels.

The space-time steering vector is given as a Kronecker product of the temporal and spatial steering vectors, denoted as $\mathbf{v}(\phi_{m,n}, f_{m,n}) = \mathbf{v}_t(f_{m,n}) \otimes \mathbf{v}_s(\phi_{m,n})$. Ignoring the impact of range ambiguities and considering a uniform linear array (ULA) with inner spacing d_a, the temporal and spatial steering vectors of the nth clutter patch are given by [1]

$$\mathbf{v}_t(f_n) = [1, \exp(j2\pi f_n), \ldots, \exp(j2\pi(N-1)f_n)]^T, \tag{2}$$

$$\mathbf{v}_s(\phi_n) = \left[1, \exp\left(\frac{j2\pi d_a}{\lambda_c} \sin\phi_n\right), \ldots, \exp\left(\frac{j2\pi(M-1)d_a}{\lambda_c} \sin\phi_n\right)\right]^T, \tag{3}$$

where $()^T$ denotes the transposition operation, and λ_c is the operate wavelength. If we stack all clutter patches' amplitudes into a vector $\boldsymbol{\sigma} = [\sigma_1, \ldots, \sigma_{N_c}]^T$, then the clutter component in (1) can be rewritten as

$$\mathbf{x}_c = \mathbf{V}\boldsymbol{\sigma}, \tag{4}$$

where $\mathbf{V} = [\mathbf{v}(f_1, \phi_1), \ldots, \mathbf{v}(f_{N_c}, \phi_{N_c})]$ denotes the clutter space-time steering matrix. Herein, the clutter covariance matrix based on (4) can

be expressed as

$$\mathbf{R}_c = E[\mathbf{x}_c \mathbf{x}_c^H] = \mathbf{V}\boldsymbol{\Sigma}\mathbf{V}^H, \tag{5}$$

where $()^H$ denotes the conjugate transposition operation and $\boldsymbol{\Sigma} = E[\boldsymbol{\sigma}\boldsymbol{\sigma}^H]$. Under the condition that the clutter patches are independent from each other, $\boldsymbol{\Sigma} = \mathrm{diag}(\mathbf{a})$, $\mathbf{a} = [a_1, \ldots, a_{N_c}]^T$ and $a_n = E[|\sigma_n|^2]$, $n = 1, \ldots, N_c$ for the statistics of the clutter patches [1, 2].

3. PROPOSED WSR-STAP ALGORITHM

In this section, we first provide an alternative method to describe the received signal. Since the clutter return is a function of the Doppler frequency and the AOA, we discretize the whole angle-Doppler plane into $N_d = \rho_d N$, $N_s = \rho_s M$ ($\rho_d, \rho_s > 1$) grids, where N_d and N_s are the number of Doppler bins and the number of angle bins, respectively [10]. Then the clutter component in (4) can be rewritten as [10]

$$\mathbf{x}_c = \boldsymbol{\Phi}\boldsymbol{\gamma}, \tag{6}$$

where $\boldsymbol{\gamma} = [\gamma_{1,1}, \gamma_{1,2}, \ldots, \gamma_{N_d,N_s}]^T$ denotes the $N_d N_s \times 1$ angle-Doppler profile with non-zero elements representing the clutter spectrum, and the $NM \times N_d N_s$ matrix $\boldsymbol{\Phi}$ is the space-time steering dictionary, as given by

$$\boldsymbol{\Phi} = [\mathbf{v}(f_1, \phi_1), \ldots, \mathbf{v}(f_1, \phi_{N_s}), \ldots, \mathbf{v}(f_{N_d}, \phi_{N_s})]. \tag{7}$$

Thus, the clutter covariance matrix can be rewritten as

$$\mathbf{R}_c = \boldsymbol{\Phi}\tilde{\boldsymbol{\Sigma}}\boldsymbol{\Phi}^H, \tag{8}$$

where $\tilde{\boldsymbol{\Sigma}} = \mathrm{diag}(\tilde{\mathbf{a}})$, $\tilde{\mathbf{a}} = [\tilde{a}_{1,1}, \tilde{a}_{1,2}, \ldots, \tilde{a}_{N_d,N_s}]^T$ and $\tilde{a}_{i,k} = E[|\gamma_{i,k}|^2]$, $i = 1, 2, \ldots, N_d$, $k = 1, 2, \ldots, N_s$. The received signal in the target range bin can be reformulated as

$$\mathbf{x} = \alpha\mathbf{s} + \boldsymbol{\Phi}\boldsymbol{\gamma} + \mathbf{n}, \tag{9}$$

where α is the target complex gain and $\mathbf{s}$ the $NM \times 1$ space-time steering vector in the target look-direction with similar formulation as $\mathbf{v}$. From (8), we observe that we can estimate the clutter covariance matrix $\mathbf{R}_c$ by estimating the statistics $\tilde{\mathbf{a}}$ first, which can be calculated via two approaches, i.e., using the snapshot in the test range bin and using snapshots from adjacent target-free range bins.

Nonetheless, both approaches can be converted into the following optimization problem known as the least absolute shrinkage and selection operator (LASSO) [13–15]

$$\hat{\boldsymbol{\gamma}} = \arg\min_{\boldsymbol{\gamma}} \|\boldsymbol{\gamma}\|_1 \quad \text{subject to} \quad \|\mathbf{x} - \boldsymbol{\Phi}\boldsymbol{\gamma}\|_2^2 \leq \epsilon, \tag{10}$$

or the basis pursuit denoising (BPDN) [9–11, 14], given as

$$\hat{\boldsymbol{\gamma}} = \arg\min_{\boldsymbol{\gamma}} \left\{ \frac{1}{2}\|\mathbf{x} - \boldsymbol{\Phi}\boldsymbol{\gamma}\|_2^2 + \kappa\|\boldsymbol{\gamma}\|_1 \right\}, \tag{11}$$

where $\|\cdot\|_p$ $(p = 1, 2)$ denotes the l_p-norm, κ the positive regularization parameter that provides a tradeoff between the l_1-norm and l_2-norm, and ϵ the noise error allowance.

By inspecting (10) and (11), there are two aspects should be noted. One is that the entries in $\boldsymbol{\gamma}$ usually do not satisfy $|\gamma_{i,k}| \leq 1$, $i = 1, 2, \ldots, N_d$, $k = 1, 2, \ldots, N_s$, which means that the l_1-norm is not the convex envelope of the l_0-norm function. In another word, the l_1-norm is not a good convex approximation of l_0-norm. The other aspect is that the nonzero entries of the angle-Doppler profile $\boldsymbol{\gamma}$ are random variables, which results in different values of the same nonzero entry from different snapshots.

With regard to the above two aspects, motivated by the work in [18], we can employ a weighted l_1-norm penalty to counteract the influence of the signal magnitude on the l_1 penalty function. Thus, we have the following optimizations

$$\hat{\boldsymbol{\gamma}} = \arg\min_{\boldsymbol{\gamma}} \|\mathbf{W}\boldsymbol{\gamma}\|_1 \quad \text{subject to} \quad \|\mathbf{x} - \boldsymbol{\Phi}\boldsymbol{\gamma}\|_2^2 \leq \epsilon, \tag{12}$$

or

$$\hat{\boldsymbol{\gamma}} = \arg\min_{\boldsymbol{\gamma}} \left\{ \frac{1}{2}\|\mathbf{x} - \boldsymbol{\Phi}\boldsymbol{\gamma}\|_2^2 + \kappa\|\mathbf{W}\boldsymbol{\gamma}\|_1 \right\}, \tag{13}$$

where $\mathbf{W}$ is a diagonal matrix with positive elements $W_{1,1}$, $W_{1,2}$, …, W_{N_d,N_s} on the diagonal and zeros elsewhere. The question that arises is how to design the weight matrix $\mathbf{W}$. Intuitively, the weights should change with the signal environments. Moreover, they should be inversely proportional to the true signal magnitude. However, it is hard to obtain the exact values of the true signal magnitude and should be estimated from the received snapshots. Several authors in [19] try to design the penalty weights using the Capon spectrum estimated from the snapshots to estimate the target's DOA. In this paper, we can simply modified this idea and apply that to the STAP applications. Since the snapshots are limited for STAP problem, especially in nonhomogeneous environments, we estimate the Capon's spectrum using the diagonal loading technique, as given by

$$Q_{m,n} = \frac{1}{|\mathbf{v}(f_m, \phi_n)^H \hat{\mathbf{R}}_{\text{capon}}^{-1} \mathbf{v}(f_m, \phi_n)|}, \tag{14}$$

where $m = 1, 2, \ldots, N_d$, $n = 1, 2, \ldots, N_s$, $\hat{\mathbf{R}}_{\text{capon}} = \frac{1}{L'}\sum_{l=1}^{L'} \mathbf{x}_l \mathbf{x}_l^H + \delta\mathbf{I}$, L' is the number of snapshots to estimate the Capon's spectrum and δ is

the diagonal loading factor. Then the penalty weights can be designed as $W_{m,n} = 1/Q_{m,n}$. But this kind approach requires a large number of snapshots to obtain a good Capon spectrum and the accuracy will degrade when the snapshots do not satisfy IID condition. Furthermore, the Capon spectrum needs a matrix inverse resulting in expensive computational complexity. To overcome the above problems, we devise the l_1-norm penalty weights for each snapshot using its own Fourier spectrum computed by the current snapshot, which is given by

$$W_{m,n} = \frac{1}{|\mathbf{v}(f_m, \phi_n)^H \mathbf{x}|}, \tag{15}$$

where $m = 1, 2, \ldots, N_d$, $n = 1, 2, \ldots, N_s$. It is seen that the proposed algorithm can be applied to arbitrary situations, unlike the approach in [10] requiring to know the exact clutter bridge in the angle-Doppler plane. The above optimization problems can directly use an optimization toolbox called CVX Matlab Toolbox provided by [20].

For the weighted D3SR-STAP using the snapshot only in the test range bin, we can estimate the angle-Doppler profile by solving (12) or (13) with the Fourier spectrum or the Capon's spectrum. Then the clutter covariance matrix $\hat{\mathbf{R}}_c$ is computed according to the approach in [15] after excluding the signal components by using some prior knowledge of the signal under detection. Specially, it first determines the signal of interest area Ω in the anlge-Doppler plane using the prior knowledge of the target signal (it is usually assumed known in STAP problem) [15]. And then the clutter covariance matrix can be estimated by

$$\hat{\mathbf{R}}_c = \sum_{i=1,k=1}^{N_d,N_s} \hat{a}_{i,k} \mathbf{v}(f_{d,i}, \phi_k) \mathbf{v}^H(f_{d,i}, \phi_k), \quad i, k \notin \Omega. \tag{16}$$

Finally, the STAP filter weights can be calculated via the Capon's optimal filter, as given by

$$\hat{\mathbf{w}} = \mu \big[\hat{\mathbf{R}}_c + \hat{\sigma}_n^2 \mathbf{I}\big]^{-1} \mathbf{s}. \tag{17}$$

where μ is a constant which does not affect the SINR performance, $\hat{\sigma}_n^2$ is the estimated noise power level, and $\mathbf{I}$ denotes the identity matrix.

For the weighted SR-STAP using multiple snapshots from adjacent range bins, we can also estimate the angle-Doppler profile by solving (12) or (13) with the Fourier spectrum or the Capon's spectrum. Then the parameter $\hat{\bar{a}}_i$ can be calculated by

$$\hat{\bar{a}}_i = \frac{1}{L} \sum_{l=1}^{L} |\hat{\gamma}_{l;i}|^2, \quad l = 1, 2, \ldots, L, \tag{18}$$

where L is the number of training snapshots and $\hat{\boldsymbol{\gamma}}_l$ the estimated angle-Doppler profile for the lth snapshot. Substituting the estimated parameter $\hat{\hat{\mathbf{a}}}$ into (8), we can obtain the estimated clutter covariance matrix. At last, the STAP filter weights can also be computed by (17).

4. NUMERICAL EXAMPLES

We assess the weighted SR-STAP and D3SR-STAP algorithms by showing the SINR performance and probability of detection performance using simulated radar data. The weighted SR-STAP and D3SR-STAP using the Capon's spectrum are shortened as CWSR-STAP and D3CWSR-STAP, and the weighted SR-STAP and D3SR-STAP using the Fourier spectrum are shortened as FWSR-STAP and D3FWSR-STAP. If there are no special illustrations, the simulated scenarios are supposed with the following parameters: side-looking ULA with half length inner spacing, uniform transmit pattern, $M = 8$, $N = 8$, carrier frequency of $f_c = 450\,\text{MHz}$, pulse repetition frequency (PRF) of $f_r = 300\,\text{Hz}$, platform velocity of $v_p = 50\,\text{m/s}$, platform height of $h_p = 9000\,\text{m}$, clutter-to-noise ratio (CNR) of 50 dB, and unitary thermal noise power. For all algorithms, the noise allowance parameter ϵ, the diagonal loading factor δ and $\hat{\sigma}_n^2$ are both set to the thermal noise power level. The selection of the size of the discretized angle-Doppler grids $N_d N_s$ plays an important role in the proposed technique. The details of the discretization is discussed in [14]. Generally, the larger the size of discretized angle-Doppler grids, the better the accuracy of the model $\mathbf{x}_c = \boldsymbol{\Phi}\boldsymbol{\gamma}$ to represent $\mathbf{x}_c = \mathbf{V}\boldsymbol{\sigma}$. But because of the existence of the noise and the high correlation of the columns of space-time steering dictionary $\boldsymbol{\Phi}$, the recovered accuracy will not improve much when the size of discretized angle-Doppler grids is over some value. While the computational complexity will become higher with the increase of the size of the discretized angle-Doppler grids. Thus it is a trade-off to select a suitable size of the discretized angle-Doppler grids to obtain both good performance and acceptable computational complexity. It is concluded that $\rho_d = \rho_s = 4$ is a good choice for the scenarios above [14].

4.1. Performance of Proposed Weighted SR-STAP Algorithms

In the first example, we access the SINR performance against the snapshots of the CWSR-STAP algorithm, the FWSR-STAP algorithm and the conventional SR-STAP algorithm. The algorithms are simulated over 10 snapshots and the target is located at boresight (0°)

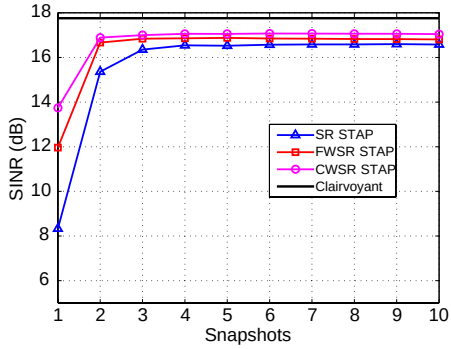

Figure 1. SINR performance against the number of snapshots of the FWSR-STAP, CWSR-STAP and SR-STAP algorithms.

with Doppler frequency of 100 Hz and the signal-to-noise ratio (SNR) of 0 dB. The output SINR is defined by

$$\mathrm{SINR} = 10\log_{10}\frac{\left|\hat{\mathbf{w}}^H\mathbf{s}\right|^2}{\left|\hat{\mathbf{w}}^H\mathbf{R}\hat{\mathbf{w}}\right|}. \tag{19}$$

where $\mathbf{R}$ is the true clutter plus noise covariance matrix. Here, 100 independent Monte Carlo simulations are carried out to obtain the average performance. The Capon's spectrum is estimated using $L' = 4$ snapshots for the CWSR-STAP algorithm. The curves in Figure 1 show that the weighted SR-STAP algorithms have a faster convergence and a better steady-state performance than the conventional SR-STAP algorithm. This is because this kind of algorithms can provide a better clutter covariance matrix estimate through the weighted l_1-norm penalty scheme. Although the FWSR-STAP algorithm has a lower steady-state performance than the CWSR-STAP algorithm, it should be noted that we use only the current snapshot to design the penalty weights in the FWSR-STAP algorithm, while in the CWSR-STAP algorithm it requires multiple snapshots and a good diagonal loading factor. Furthermore, the l_1-norm penalty weights in the FWSR-STAP algorithm has a much lower complexity than the CWSR-STAP algorithm, which requires a matrix inverse operation in (14).

In the second example, we evaluate the SINR performance against the Doppler frequency of the weighted SR-STAP algorithms. The potential target Doppler frequency space from -150 to 150 Hz is examined and other target's parameters are the same as the first example. We consider three different scenarios: (i) the ideal case where the space-time clutter plus noise snapshots are generated through (1) with no range ambiguity; (ii) the temporal decorrelation case where we

consider the inner clutter motion (ICM); (iii) the spatial decorrelation case where we consider the channel mismatch. The ICM can be formulated as a general model that proposed by J. Ward in [1], which is suitable over the water scenario. The temporal autocorrelation of the fluctuations is Gaussian in shape with the form:

$$\zeta(m) = \exp\left\{-\frac{8\pi^2\sigma_v^2 T_r^2}{\lambda_c^2}m^2\right\}, \tag{20}$$

where T_r is the the pulse repetition interval and σ_v the velocity standard deviation (in the example. We set $\sigma_v = 0.5$ corresponding to a serious clutter Doppler spreading situation). With regard to the channel mismatch, we only consider the angle-independent array errors described in [13], i.e., the amplitude and phase errors are modeled as a narrowband case as follows:

$$p(\delta_{\epsilon_a}) = \begin{cases} \frac{1}{\Delta\epsilon_a} & \text{for} \quad 0 \le \delta_{\epsilon_a} \le \Delta\epsilon_a \\ 0 & \text{elsewhere} \end{cases}, \tag{21}$$

and

$$p(\delta_{\epsilon_p}) = \begin{cases} \frac{1}{\Delta\epsilon_p} & \text{for} \quad -\frac{\Delta\epsilon_p}{2} \le \delta_{\epsilon_p} \le \frac{\Delta\epsilon_p}{2} \\ 0 & \text{elsewhere} \end{cases}, \tag{22}$$

where $p(\delta_{\epsilon_a})$ and $p(\delta_{\epsilon_p})$ are the pdfs (uniform) associated with the amplitude and phase errors respectively. In the example, we set

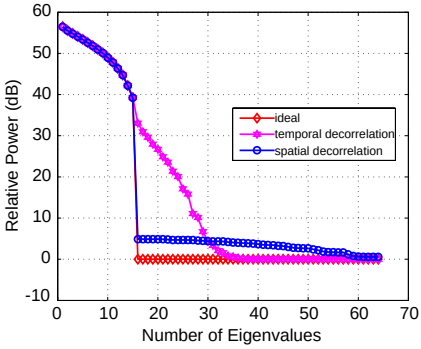

Figure 2. Clutter eigenspectrum with three different cases: (i) the ideal case; (ii) the temporal decorrelation case; (iii) the spatial decorrelation case.

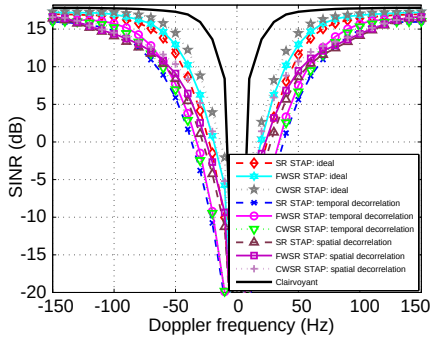

Figure 3. SINR performance against the target Doppler frequency of the FWSR-STAP, CWSR-STAP and SR-STAP algorithms with three different cases: (i) the ideal case; (ii) the temporal decorrelation case; (iii) the spatial decorrelation case.

$\Delta\epsilon_a = 0.01$ and $\Delta\epsilon_p = 1^\circ$. The clutter eigenspectrum (which is computed by taking an eigenvalue decomposition to the true clutter-noise covariance matrix) about these three cases are depicted in Figure 2. It is illustrated that the spatial and temporal decorrelation will lead to the increase of clutter rank.

As shown in Figure 3, we set the number of the training snapshots 4 for the FWSR-STAP algorithm, the CWSR-STAP algorithm and the SR-STAP algorithm, and the clairvoyant SINR performance is computed using the true clutter plus noise covariance matrix under the ideal case [2]. The plots illustrate that the weighted SR-STAP algorithms provide a narrower clutter notch and a better SINR performance compared with the conventional SR-STAP algorithm in all three cases. One also notes that the FWSR-STAP provides a worse performance than the CWSR-STAP in both ideal and spatial decorrelation cases, but obtains a better performance in temporal decorrelation case. For better understanding of these results, we take the estimated Fourier spectrum, estimated Capon's spectrum and estimated angle-Doppler profiles of one snapshot for example in Figure 4 and Figure 5 (here, we focus on the results of the ideal case and the temporal decorrelation case). Figure 4 shows that the Capon's spectrum exhibits a much better estimation than the Fourier spectrum resulting in a better penalty weights designing. That is why the CWSR-STAP can obtain a better performance than the FWSR-STAP algorithm in the ideal case. For the temporal decorrelation case, the true clutter spectrum becomes much broader due to the Doppler spreading of the clutter, e.g., Figure 5(c). In this case, the Capon's spectrum estimated only by 4 snapshots, e.g., Figure 5(b), is less sufficient even compared with the Fourier spectrum estimated by the current snapshots, e.g., Figure 5(a). Thus, the performance of the CWSR-STAP is worse than that of the FWSR-STAP algorithm. Above conclusions are also can be observed by Figures 4(c)–(e) and Figures 5(c)–(e).

From Figure 3, we also note that the performance of the algorithms degrades when in presence of spatial or temporal decorrelations. That is because the spatial or temporal decorrelations will lead to the clutter rank increase, e.g., Figure 2. Herein, it requires a wider clutter notch or, equivalently, more adaptive degrees of freedom for effective cancelation [1].

In the third example, we present the probability of detection performance (P_d) versus the target SNR for the CWSR-STAP, the FWSR-STAP and the SR-STAP algorithms. The false alarm rate P_{fa} is set to 10^{-3} and for simulation purposes threshold and P_d estimates are based on 5,000 samples from the target absence and presence

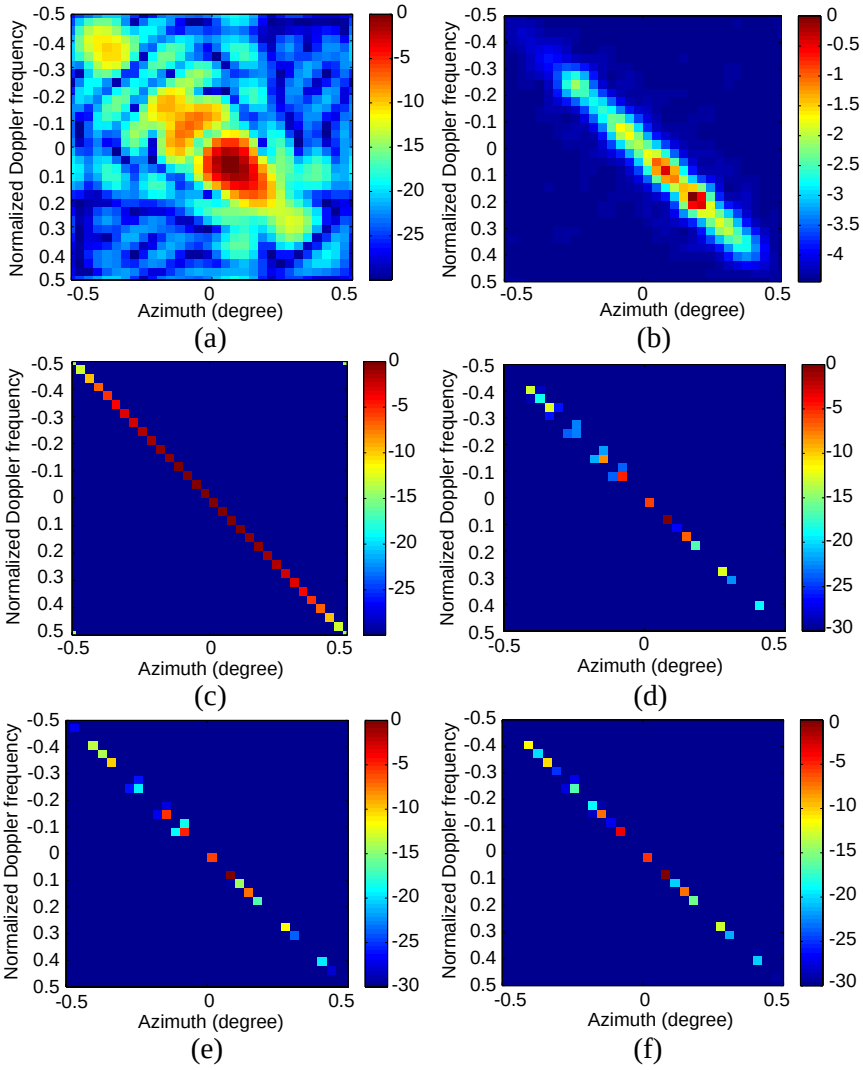

Figure 4. Estimated Fourier spectrum, Capon's spectrum and angle-Doppler profiles of one snapshot in the ideal case. (a) Estimated Fourier spectrum using the current snapshot. (b) Estimated Capon's spectrum using 4 snapshots with diagonal loading factor equating to the thermal noise power. (c) Capon's spectrum using the true clutter plus noise covariance matrix. (d) Estimated angle-Doppler profile using the SR-STAP. (e) Estimated angle-Doppler profile using the FWSR-STAP. (f) Estimated angle-Doppler profile using the CWSR-STAP.

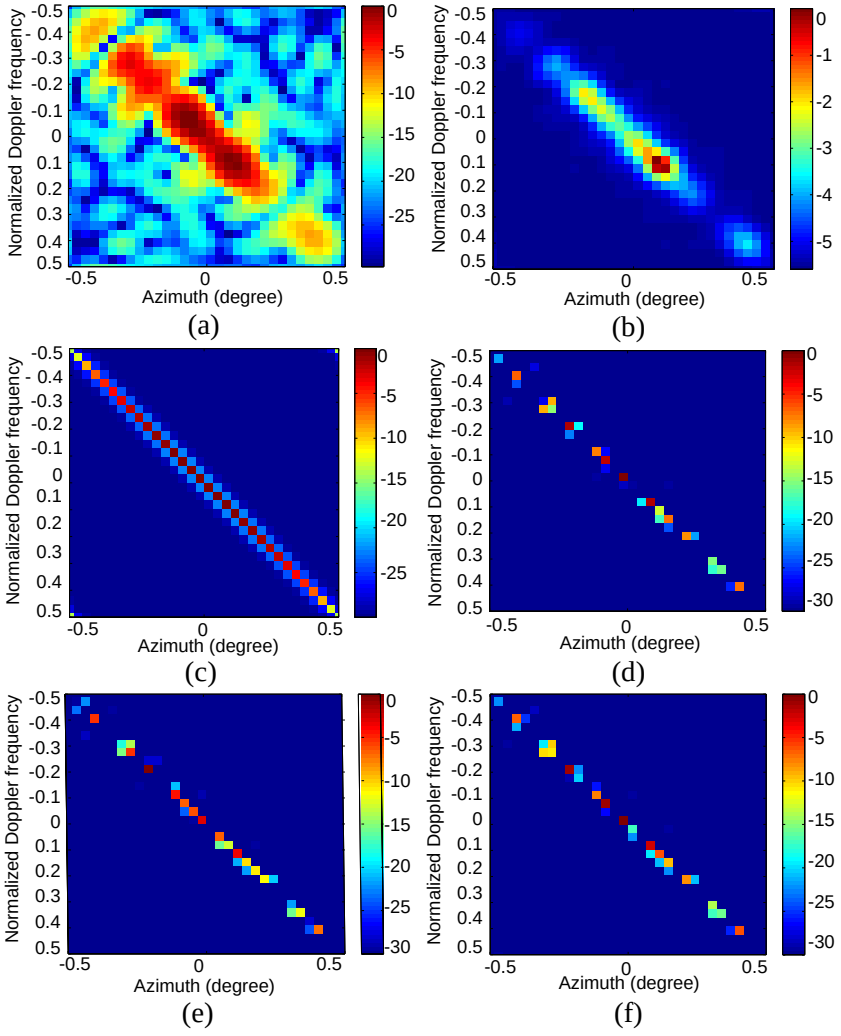

Figure 5. Estimated Fourier spectrum, Capon's spectrum and angle-Doppler profiles of one snapshot in the temporal decorrelation case. (a) Estimated Fourier spectrum using the current snapshot. (b) Estimated Capon's spectrum using 4 snapshots with diagonal loading factor equating to the thermal noise power. (c) Capon's spectrum using the true clutter plus noise covariance matrix. (d) Estimated angle-Doppler profile using the SR-STAP. (e) Estimated angle-Doppler profile using the FWSR-STAP. (f) Estimated angle-Doppler profile using the CWSR-STAP.

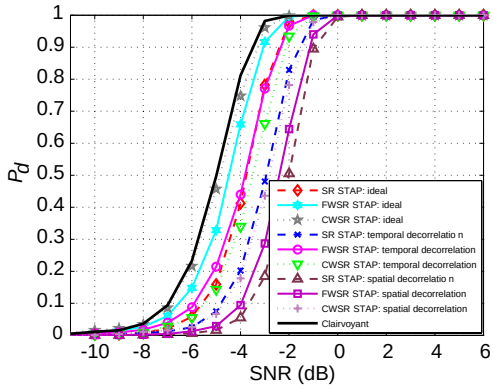

Figure 6. P_d versus SNR with $P_{fa} = 10^{-3}$ of the FWSR-STAP, CWSR-STAP and SR-STAP algorithms with three different cases: (i) the ideal case; (ii) the temporal decorrelation case; (iii) the spatial decorrelation case.

respectively. We suppose the target is injected in the boresight (0°) with Doppler frequency 100 Hz (the normalized Doppler frequency is 0.33). The other parameters are the same as those in the second example. The curves plotted in Figure 6 illustrate that the weighted SR-STAP algorithms provide suboptimal detection performance, but remarkably, obtain a higher detection rate than the conventional SR-STAP at an SNR level from −8 dB to 0 dB. It is also seen that the performance of the FWSR-STAP algorithm is worse than that of the CWSR-STAP algorithm in both ideal case and spatial decorrelation case, but better than it in the temporal decorrelation case.

4.2. Performance of Proposed Weighted D3SR-STAP Algorithms

In this subsection, we focus on the performance evaluation of the weighted D3SR-STAP algorithms. Firstly, like the second example in the Section 4.1, it plots the SINR performance against the target Doppler frequency in Figure 7 (the simulation scenarios are the same as those in the second example in the Section 4.1). Traditional measurement (e.g., SINR in (19)) needs to know the true clutter statistical information to evaluate this metric, which is unknown in the D3 case. Thus, we simply calculate the output SINR as [15]

$$\mathrm{SINR} = 10\log_{10}\frac{\sum_{p=1}^{N_{nmc}}\left|\hat{\mathbf{w}}_p^H\mathbf{s}\right|^2}{\sum_{p=1}^{N_{nmc}}\left|\hat{\mathbf{w}}_p^H(\mathbf{x}_{c,p}+\mathbf{n}_p)\right|^2}, \tag{23}$$

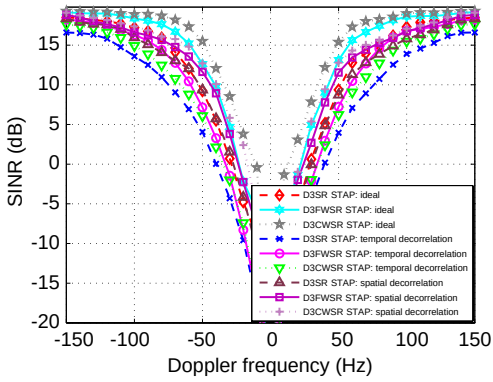

Figure 7. SINR performance against the Doppler frequency of the D3FWSR-STAP, D3CWSR-STAP and D3SR-STAP algorithms with three different cases: (i) the ideal case; (ii) the temporal decorrelation case; (iii) the spatial decorrelation case.

where N_{nmc} is the number of independent Monte Carlo runs (here, $N_{nmc} = 1000$), $\mathbf{s}$ the space-time steering vector of the moving target, and $\mathbf{x}_{c,p} + \mathbf{n}_p$ the clutter plus noise return in the test range bin. From the figure, the similar conclusions as those in Section 4.1 the second and third examples can also be obtained, i.e., (i) the weighted D3SR-STAP algorithms outperform the conventional D3SR-STAP algorithm; (ii) the D3FWSR-STAP provides worse performance than the D3CWSR-STAP algorithm in both ideal case and spatial decorrelation case, but better than it in the temporal decorrelation case. One note that the improvement of SINR performance between the weighted D3SR-STAP algorithms and conventional D3SR-STAP algorithm is greater than that between the weighted D3SR-STAP algorithms and conventional SR-STAP algorithm. That is why the weighted algorithms can obtain a faster convergence than the conventional algorithm. Moreover, it should point out that the performance of the D3FWSR-STAP, D3CWSR-STAP or D3SR-STAP is better than that of the FWSR-STAP, CWSR-STAP or SR-STAP using only one snapshot, which can be observed from the Figure 1 and Figure 7 (where 18.6 dB in the D3FWSR-STAP, 19.0 dB in the D3CWSR-STAP and 17.2 dB in the D3SR-STAP beat 12 dB in the FWSR-STAP, 13.8 dB in the CWSR-STAP and 8.3 dB in the SR-STAP when the target Doppler frequency is 100 Hz in the ideal case). This is because the weighted SR-STAP algorithms and the SR-STAP belong to a class of stochastic methods which rely on training data to estimate the statistics of the interference in order to null interferers, while the weighted D3SR-

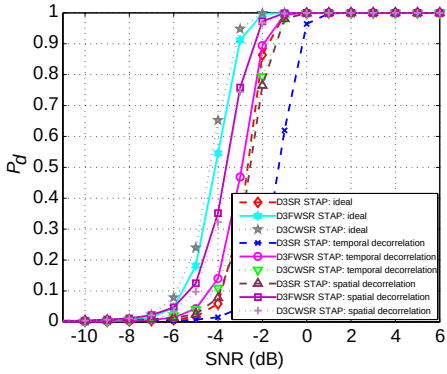

Figure 8. P_d versus SNR with $P_{fa} = 10^{-3}$ of the D3FWSR-STAP, D3CWSR-STAP and D3SR-STAP algorithms with three different cases: (i) the ideal case; (ii) the temporal decorrelation case; (iii) the spatial decorrelation case.

Table 1. Average running time (s) for recovering one angle-doppler profile.

Schemes	Ideal case	Temporal decorrelation case	Spatial decorrelation case
SR Scheme	7.1402	7.0182	7.0952
FWSR Scheme	7.1160	6.8539	6.8597
CWSR Scheme	7.5347	7.4607	7.5204

STAP algorithms and the D3SR-STAP algorithm belong to a class of deterministic methods, which operate on a snapshot-by-snapshot basis to determine the adaptive weights [2]. It is hard to obtain a good statistics of the interference using only one snapshot from the adjacent range bins even though the interference satisfies the IID condition in the weighted SR-STAP algorithms or the SR-STAP algorithms. However, in the weighted D3SR-STAP algorithms and the D3SR-STAP algorithm, a deterministic method provides an estimate which comes closer to the Cramer-Rao bound than do the results provided by a stochastic methodology (see [2], Chapter 12).

Figure 8 illustrates the P_d versus the SNR performance for the weighted D3SR-STAP algorithms and the conventional D3SR-STAP algorithm. The scenario parameters are the same as those in the third example in the Section 4.1. The figure shows that the D3FWSR-

STAP algorithm provides approximately detection performance as the D3CWSR-STAP algorithm, but obtains a much higher detection rate than the D3SR-STAP algorithm at an SNR from −6 dB to 1 dB. Furthermore, compared with the results in Figure 7 and Figure 8, we observe that the performance degradation of the D3SR-STAP algorithm is larger than those of the weighted D3SR-STAP algorithms when in presence of temporal decorrelation. Thus, from this point of view, the weighted D3SR-STAP algorithms exhibit a better robustness to the ICM than the conventional algorithm.

To provide a further investigation of the performance of the the l_1-norm penalty weighted scheme, we depict the average running time (second, s) for recovering one angle-Doppler profile in Table 1. Here, our simulations are operated on a standard desktop computer with a 2.60 GHz CPU and 2 GB of memory. It is seen that the CWSR scheme has the highest computational complexity compared with the FWSR scheme and SR scheme. One should also note that the FWSR scheme even has a lower computational complexity compared with the SR scheme, why this happens requiring a further investigation. In addition, the average running time for recovering one angle-Doppler profile using CVX toolbox is very high in airborne radar applications, which makes this kind of algorithms hard to realization. Thus, to exploit the advantages, i.e., the fast convergence and high performance of weighted type algorithms, it is worthy designing fast weighted SR algorithms in the future work.

5. CONCLUSION AND DISCUSSION

In this paper, we have presented novel weighted SR-STAP and D3SR-STAP algorithms for airborne radar applications. The proposed algorithms utilize a weighted l_1-norm penalty based on the Capon's spectrum and the Fourier spectrum to further enforce the sparsity and approximate the original l_0-norm. Simulation results have shown that the FWSR-STAP and D3FWSR-STAP algorithms provide approximately performance and lower computational complexity compared with the CWSR-STAP and D3CWSR-STAP algorithms, but remarkably outperform the conventional SR-STAP and D3SR-STAP algorithms in terms of the SINR steady-state performance, the convergence speed and the detection performance.

Further investigation is required on several issues: (i) it needs to devise the fast weighted SR algorithms; (ii) the effect of nonhomogeneous factors to the proposed methods (iii) the testing of the proposed methods on real radar data.

ACKNOWLEDGMENT

This work is funded in part by the National Natural Science Foundation of China (61171133 and 61025006), and National Natural Science Foundation of Hunan Province of China (11zz1010).

REFERENCES

1. Ward, J., "Space-time adaptive processing for airborne radar," Technical Report 1015, MIT Lincoln laboratory, Lexington, MAvol, Dec. 1994.
2. Klemm, R., *Applications of Space-time Adaptive Processing,* The Institution of Electrical Engineers, London, UK, 2004.
3. Guerci, J. R., *Space-time Adaptive Processing for Radar,* Artech House, 2003.
4. Gong, Q. Y. and Z. D. Zhu, "Study STAP algorithm on interference target detect under nonhomogeneous environment," *Progress In Electromagnetics Research*, Vol. 99, 211–224, 2009.
5. Liu, Y. P. and Q. Wan, "Total difference based partial sparse LCMV beamformer," *Progress In Electromagnetics Research Letters*, Vol. 18, 97–103, 2010.
6. Zhang, Y., Q. Wan, and A. M. Huang, "Localization of narrow band sources in the presence of mutual coupling via sparse solution finding," *Progress In Electromagnetics Research*, Vol. 86, 243–257, 2008.
7. Yang, M. and G. Zhang, "Compressive sensing based parameter estimation for monostatic MIMO noise radar," *Progress In Electromagnetics Research Letters*, Vol. 30, 133–143, 2012.
8. Liu Z., X. Wei, and X. Li, "Adaptive clutter suppression for airborne random pulse repetition interval radar based on compressed sensing," *Progress In Electromagnetics Research*, Vol. 128, 291–311, 2012.
9. Maria, S. and J. J. Fuchs, "Application of the global matched filter to STAP data an efficient algorithmic approach," *Proc. IEEE Int. Conf. Acoust. Speech and Signal Process.*, 14–19, 2006.
10. Selesnick, I. W., S. U. Pillai, K. Y. Li, and B. Himed, "Angle-doppler processing using sparse regularization," *Proc. IEEE Int. Conf. Acoust. Speech and Signal Process.*, 2750–2753, 2010.
11. Parker, J. T. and L. C. Potter, "A Bayesian perspective on sparse regularization for STAP post-processing," *Proc. IEEE Radar Conf.*, 1471–1475, May 2010.

12. Li, J., X. Zhu, P. Stoica, and M. Rangaswamy, "High resolution angle-Doppler imaging for MTI radar," *IEEE Trans. Aerosp. Electron. Syst.*, Vol. 46, No. 3, 1544–1556, Jul. 2010.
13. Sun, K., H. Zhang, G. Li, H. Meng, and X. Wang, "A novel STAP algorithm using sparse recovery technique," *Proc. IGARSS*, 336–339, 2009.
14. Yang, Z., Z. Liu, X. Li, and L. Nie, "Performance analysis of STAP algorithms based on fast sparse recovery techniques," *Progress In Electromagnetics Research B*, Vol. 41, 251–268, 2012.
15. Sun, K., H. Meng, Y. Wang, and X. Wang, "Direct data domain STAP using sparse representation of clutter spectrum," *Signal Process.*, Vol. 91, No. 9, 2222–2236, 2011.
16. Yang, Z., R. C. de Lamare, and X. Li, "L_1-regularized STAP algorithms with a generalized sidelobe canceler architecture for airborne radar," *IEEE Trans. Signal Process.*, Vol. 60, No. 2, 674–686, 2012.
17. Yang, Z., R. C. de Lamare, and X. Li, "Sparsity-aware STAP algorithms for airborne radar based on conjugate gradient techniques," *Proc. Sensor Signal Process. for Defence Conf.*, London, UK, 2011.
18. Candes, E. J., M. B. Wakin, and S. P. Boyd, "Enhancing sparsity by reweighted l_1 minimization," *J. Fourier Anal. Applicat.*, Vol. 14, Nos. 5–6, 877–905, 2008.
19. Xu, X., X. Wei, and Z. Ye, "DOA estimation based on sparse signal recovery utilizing weighted l_1-norm penalty," *IEEE Signal Process. Letters*, Vol. 19, No. 3, 155–158, 2012.
20. http://www.stanford.edu/ boyd/cvx.